

Ultrafast dynamics in a nanocage of enzymes: Solvation and fluorescence resonance energy transfer in reverse micelles

Parijat Majumder^a, Rupa Sarkar^a, Ajay Kumar Shaw^a, Anjan Chakraborty^b,
Samir Kumar Pal^{a,*}

^a C.K. Majumdar Laboratory, S.N. Bose National Centre for Basic Sciences, Block JD, Sector III, Salt Lake, Kolkata 700 098, India

^b Department of Chemistry, Indian Institute of Technology, Kharagpur, India

Received 11 December 2004; accepted 19 April 2005

Available online 6 June 2005

Abstract

In this contribution we report studies of the nature of solvation and resonance energy transfer processes in a reverse micelle (RM) upon encapsulation of a digestive enzyme, α -chymotrypsin (CHT). We have used one donor, Coumarin 500 (C500), and three acceptors Rhodamine 123 (R123, cationic), ethidium bromide (EtBr, cationic), and Merocyanine 540 (MC540, anionic). By selectively exciting the donor at the surface of the RM with a proper excitation wavelength we have examined solvation dynamics in the microenvironment. The solvation correlation function in the RM without CHT exhibits single-exponential decay with time constant ~ 660 ps, which is similar to that of the CHT-included RM. However, in the case of CHT-included RM ($w_0 = 10$), the time-resolved anisotropy and spectral linewidth analysis of the surface-bound donor reveal the existence of an annular aqueous channel of thickness ~ 2.5 Å between the enzyme surface and the inner surface of the RM. The aqueous channel is a potential host for the water-soluble substrate and also is involved in maintaining the proper functionality of RM encapsulated CHT. The studies use both steady-state and time-resolved fluorescence resonance energy transfer (FRET) techniques to measure donor–acceptor distances in the RM and also emphasize the danger of using steady-state fluorescence quenching as a method in careful estimation of the distances. The local geometrical restriction on the donor and acceptor molecules was estimated from time-resolved polarization (anisotropy) measurements. The time-resolved anisotropy of the donor and acceptor molecules also revealed significant randomization of the relative orientation of transition dipoles of the donor and acceptor, justifying the use of $2/3$ as the value of the orientation factor κ^2 . These studies attempt to elucidate the excellence of the RM as a nanohost of biological macromolecules.

© 2005 Elsevier Inc. All rights reserved.

Keywords: Fluorescence resonance energy transfer (FRET); Solvation dynamics; Time-resolved anisotropy; Reverse micelle; α -Chymotrypsin; Nanocage; Enzyme; Temporal spectral width; TRES; TRANES

1. Introduction

Water molecules in the close vicinity of biological macromolecules (hydration) are particularly important for the function of biomolecular recognition [1]. Modulating the number of water molecules available to an enzyme for modifying its activity has opened a new field of research of

paramount interest [2–4]. In order to explore the interplay between hydration and enzymatic structure/function it has become necessary to design novel experimental systems. Several systems, such as protein films at various levels of hydration [5], have been developed. However, two systems have widely evolved in which the relation between water and enzymes can be experimentally approached. One involves the entrapment of enzymes in the reverse micelle [6–8] and the other the dispersion of enzymes in nonpolar solvents [9,10]. These two nonconventional systems have a common factor: the amount of water available to enzymes

* Corresponding author. Fax: +91 33 2335 3477.
E-mail address: skpal@bose.res.in (S.K. Pal).

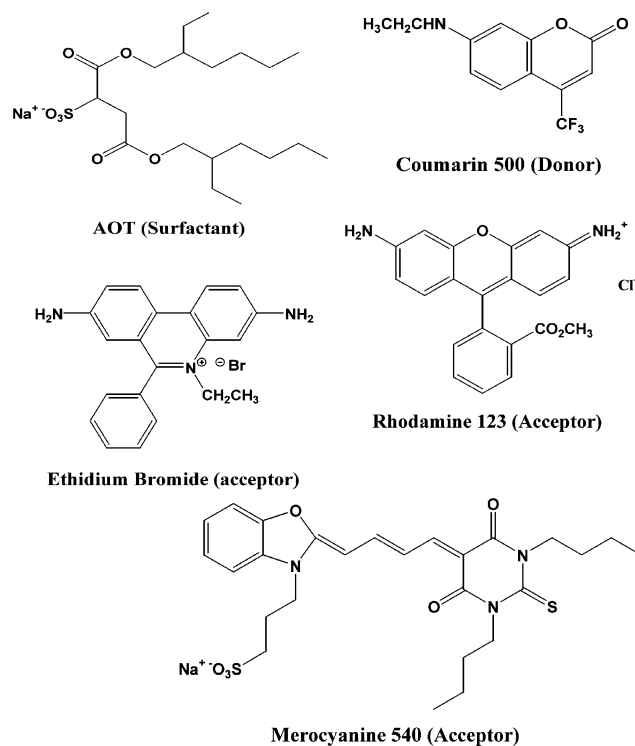
can be controlled and made much lower than in the usual biological systems.

Reverse micelles (RM) are tiny aqueous droplets surrounded and stabilized by a monolayer of surfactant molecules and dispersed in a water-immiscible organic solvent [4]. A well-known direct relationship exists between the radius of RM of AOT (surfactant; aerosol OT) in isooctane (nonpolar solvent) and their degree of hydration, w_0 , described by

$$r_m (\text{\AA}) = 2w_0, \quad (1)$$

where r_m is the radius of the water pool in \AA and $w_0 = [\text{water}]/[\text{AOT}]$. At present, reverse micellar microemulsions are widely used as organic media for performing biocatalysis. They have been associated with the idea of a “nanocage” or “microreactor” [6–8] where enzyme can be sheltered and protected from the solvent detrimental effects. In some particular cases it is possible to solubilize enzymes in RM without the loss of the native structures of those enzymes [11]. In a recent study from this group [4], the catalytic activity of an enzyme α -chymotrypsin (CHT) was measured in the RM with various degrees of hydration and was found to be retarded by at least two orders of magnitude relative to that of the free enzyme in buffer solutions. In the experimental investigation [4] the reactions were studied at those values of w_0 where the native structure of CHT was preserved [11]. The work inferred that the locations of the enzyme and substrate were important factors in the observed enzymatic activity of CHT in the RM. The present study focuses on the location of small molecules (substrate mimics) with different charges in a RM with and without inclusion of CHT.

In this work we used fluorescence resonance energy transfer (FRET) technique to assess distances of three acceptor probe molecules (two cationic and one anionic) from the surface of the RM before and after encapsulation of CHT. The energy donor, Coumarin 500 (C500; neutral), was selectively excited at the RM surface by using specific excitation wavelength. The energy acceptors Rhodamine 123 (R123; cationic), ethidium bromide (EtBr; cationic), and Merocyanine 540 (MC540; anionic), being extremely hydrophilic, are completely insoluble in the nonpolar phase (isooctane) of the RM. The molecular structure of the donor, the acceptors, and the surfactant AOT are shown in Scheme 1. Upon selective excitation, the donor C500 at the RM surface undergoes FRET to the acceptors in the aqueous phase of the RM. By observing the picosecond-to-nanosecond dynamics of non-radiative energy transfer of the donor in the RM without and with CHT, we elucidate locations of the charged acceptors with respect to the anionic inner surface of the RM. In order to unravel the change in the environmental dynamics around the donor we also studied picosecond-resolved solvation dynamics and polarization-analyzed anisotropy of the donor at the surface of the RM without and with CHT.



Scheme 1. Molecular structures of the surfactant AOT, donor Coumarin 500, and acceptors Rhodamine 123, ethidium bromide, and Merocyanine 540.

2. Material and methods

Lyophilized CHT powder was purchased from Sigma (highest grade). Isooctane (Spectrochem, 99.5%), bis-(2-ethylhexyl)-sulfosuccinate sodium salt (AOT; Fluka, 99%), Coumarin 500 (Exciton, 99.9%), Rhodamine 123 (Sigma, 99%), ethidium bromide (Molecular Probes, 99.9%), and Merocyanine 540 (Fluka, 99%) were used as received. Reverse micellar microemulsion with donor only was prepared by dissolving solid AOT in a precharacterized donor–isooctane solution. The final AOT concentration was 0.01 M. In most of our experiments the hydration level of the reverse micelle was maintained as $w_0 = 10$. The donor–acceptor complexes in the RM were prepared by mixing acceptors with donor–RM, equilibrating for 3 h and filtering the final solution. In order to avoid multiple occupancy of the acceptors in the RM, the ratio $[\text{RM}]/[\text{acceptor}]$ was maintained to be at most 1:1. For the same reason, donor concentration at the micellar surface was maintained to be lower than the concentration of the RM. The concentration of the RM at our $[\text{AOT}]$ was determined on taking the aggregation constant of AOT in isooctane to be $100 \mu\text{M}$ [12]. Inclusion of CHT in the RM was made by adding CHT powder to the RM, stirring vigorously for 3 h and filtering the solution. Concentration of the enzyme CHT samples in the aqueous solutions was determined using the supplied (by the vendor) extinction coefficient value at 280 nm, $\epsilon_{280}(1\%) = 20.4 \text{ cm}^{-1}$.

Steady-state absorption and emission were measured with a Shimadzu Model UV-2450 spectrophotometer and a

Jobin Yvon Model Fluoromax-3 fluorimeter, respectively. All transients were taken using the picosecond-resolved time-correlated single photon counting (TCSPC) technique. We used a commercially available picosecond diode laser-pumped time-resolved fluorescence spectrophotometer from IBH, UK with instrument response function (IRF) ~ 120 ps at the Indian Institute of Technology, Kharagpur, India. The picosecond excitation pulse from the diode laser was used at 405 nm. A liquid scatterer was used to measure the FWHM of the instrument response functions (IRF). The fluorescence from the sample was detected by a microchannel plate photomultiplier tube (MCP-PMT) after dispersion through a double-grating monochromator. For all transients the polarizer on the emission side was adjusted to be at 54.7° (magic angle) with respect to the polarization axis of the excitation beam.

For anisotropy measurements, emission polarization was adjusted to be parallel or perpendicular to that of the excitation and anisotropy defined as $r(t) = [I_{\text{para}} - GI_{\text{perp}}]/[I_{\text{para}} + 2GI_{\text{perp}}]$. The magnitude of G , the grating factor of the emission monochromator of the TCSPC system, was found by using a coumarin dye in methanol and following a long-time tail-matching technique [13] to be 1.5. To construct time-resolved emission spectra after the excitation pulse, we adopted the method detailed in Ref. [14]. The observed fluorescence transients were fitted using a nonlinear least-squares fitting procedure (software SCIENTIST) to a function composed of the convolution of the instrument response function with a sum of exponentials. The purpose of this fitting is to obtain the decays in an analytic form suitable for further data analysis. For each detection wavelength the transient was normalized using the steady-state spectrum. The resulting time-resolved spectra were fitted with a lognormal shape function to estimate the spectrum maximum $\nu(t)$. The temporal Stokes shift can be represented by the time dependence of the fit. By following the time-resolved emission, we constructed the hydration correlation function $C(t) = [\nu(t) - \nu(\infty)]/[\nu(0) - \nu(\infty)]$, where $\nu(0)$, $\nu(t)$, and $\nu(\infty)$ denote the observed emission energies (in wavenumbers) at times 0, t , and ∞ , respectively. For the construction of time-resolved area-normalized emission spectra (TRANES) we followed the method described in Ref. [15].

In order to estimate the fluorescence resonance energy transfer efficiency of the donor (C500) and hence to determine distances of donor–acceptor pairs, we followed the methodology described in chap. 13 of Ref. [16]. The Forster distance (R_0) is given by

$$R_0 = 0.211[\kappa^2 n^{-4} Q_D J(\lambda)]^{1/6} \text{ (in \AA)}, \quad (2)$$

where κ^2 is a factor describing the relative orientation in space of the transition dipoles of the donor and acceptor. For donor and acceptors that randomize by rotational diffusion prior to energy transfer, the magnitude of κ^2 is assumed to be $2/3$. In the present study the same assumption has been made, and it has further been justified by time-resolved

anisotropy measurements of the donor and acceptor molecules (see below). The refractive index (n) of the medium is assumed to be 1.4. Q_D , the quantum yield of the donor in the absence of acceptor is measured to be 0.46 and 0.48 respectively in the RM without and with the enzyme CHT. $J(\lambda)$, the overlap integral, which expresses the degree of spectral overlap between the donor emission and the acceptor absorption is given by

$$J(\lambda) = \frac{\int_0^\infty F_D(\lambda) \varepsilon_A(\lambda) \lambda^4 d\lambda}{\int_0^\infty F_D(\lambda) d\lambda}, \quad (3)$$

where $F_D(\lambda)$ is the fluorescence intensity of the donor in the wavelength range of λ to $\lambda + d\lambda$ and is dimensionless. $\varepsilon_A(\lambda)$ is the extinction coefficient (in $\text{M}^{-1} \text{cm}^{-1}$) of the acceptor at λ . If λ is in nm, then $J(\lambda)$ is in units of $\text{M}^{-1} \text{cm}^{-1} \text{nm}^4$.

Once the value of R_0 is known, the donor–acceptor distance (r) can easily be calculated using the formula

$$r^6 = [R_0^6(1 - E)]/E. \quad (4)$$

Here E is the efficiency of energy transfer. The transfer efficiency is measured using the relative fluorescence intensity of the donor in the absence (F_D) and presence (F_{DA}) of the acceptor. The efficiency E is also calculated from the lifetimes under these respective conditions (τ_D and τ_{DA}):

$$E = 1 - (F_{DA}/F_D), \quad (5a)$$

$$E = 1 - (\tau_{DA}/\tau_D). \quad (5b)$$

The distances measured using Eqs. (5a) and (5b) are revealed as R^S (steady state measurement) and R^{TR} (time-resolved measurement), respectively.

3. Results and discussion

3.1. Steady-state spectroscopic studies

3.1.1. Solvation and selective excitation of the donor

The donor C500 is sparingly soluble in water and shows reasonably good solubility in isoctane. In bulk water the absorption peak (400 nm) is significantly red-shifted compared to that in isoctane (360 nm). The emission peak of C500 in bulk water (500 nm) also shows a 90-nm red shift compared to that in isoctane (excitation at 350 nm). The significantly large solvatochromic effect (solvation) in the absorption and emission spectra of C500 makes the dye an attractive probe for microenvironments. As shown in Fig. 1, in isoctane C500 offers significant solubility and the absorption spectrum shows a peak at 360 nm with a shoulder at 380 nm. Upon addition of AOT ($w_0 = 10$), another shoulder (at 400 nm) appears in the absorption spectrum, which remains similar for C500 in CHT-included RM ($w_0 = 10$), indicating a population of the donor in the polar environment of the RM. The signature of the population of donor molecules in the polar environment of the RM is also evident from the difference spectrum (middle panel of Fig. 1)

of the donor in the RM ($w_0 = 10$) with respect to the donor in isooctane. From the absorption spectra it is clear that upon excitation at 400 nm, only that population of donor molecules is excited which are in the polar environment of the RM. The lower panel of Fig. 1 clearly shows the effect of excitation wavelength on the emission of the donor in the RM. The donor in the AOT/isooctane mixture shows an emission peak at 430 nm with excitation wavelength at 350 nm, indicating emission from both the population of the donor molecules in polar and nonpolar environments. Upon excitation at 400 nm the donor emission is peak-shifted to 500 nm revealing the population of donor molecules in the polar environment only. The insignificant change of absorption/emission spectra of the donor with w_0 and upon inclusion of CHT in the RM is not surprising, given the fact that

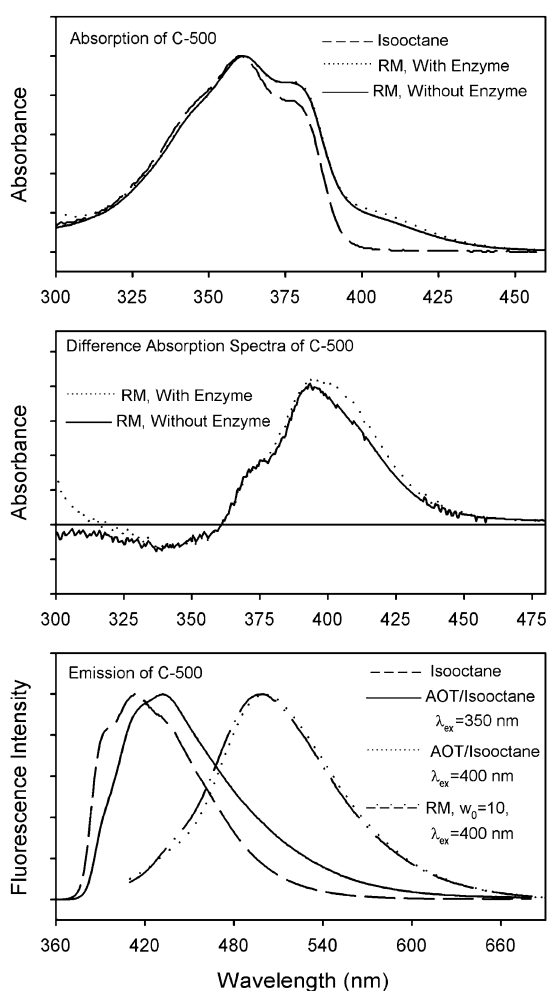


Fig. 1. Upper panel shows absorption spectra of C500 (donor) in isooctane and in the RM ($w_0 = 10$) without/with the enzyme CHT. Differential absorption spectra of C500 in the RM are shown in the middle panel. A solution of C500 in isooctane, which appears as base line in the spectra is used as reference. From the absorption spectra the signature of the C500 population in the aqueous environments at 400 nm is clearly evident. In the lower panel emission spectra of C500 in nonpolar solvent (isooctane), AOT/isooctane mixture, and the RM (without CHT) with various excitation wavelengths are shown. Note that at excitation wavelength of 400 nm, C500 in the aqueous environments of the RM would selectively be excited.

C500 is sparingly soluble in bulk water and expected to reside at the surface of the RM.

3.1.2. Quenching of the donor emission in the reverse micelle

In Fig. 2 (upper panel), the spectral overlap of the donor (C500) emission and absorption of R123 (energy acceptor) is shown. The specific property of accumulation in the mitochondria of living cells and the ability to selectively reduce clonal growth of carcinoma cells in vitro makes R123 an attractive probe in biomedical research [17]. The cationic dye R123 being extremely soluble in bulk water and completely insoluble in isooctane makes it a very good reporter of the aqueous phase of a RM. The fluorescence-quenching effects of the donor C500 in the RM without and with CHT on the acceptor R123 are shown in the middle and lower panels of Fig. 2, respectively. In the case of RM without CHT (Table 1) the quenching efficiency, measured by the ratio F_{DA}/F_D , where F_D and F_{DA} are the emission inten-

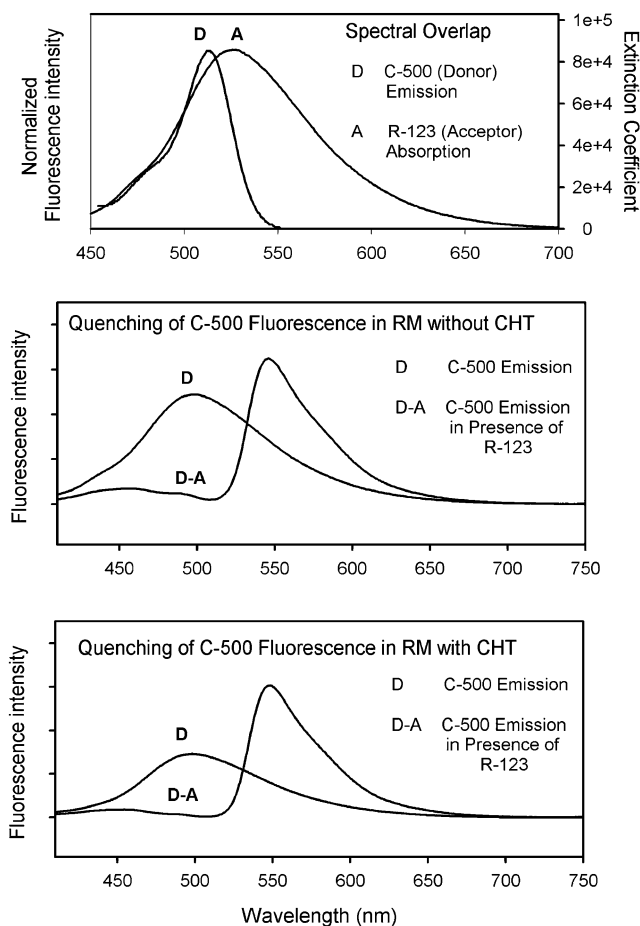


Fig. 2. The fluorescence energy-transfer processes of C500 (donor) to a cationic acceptor R123 in the RM as evidenced from steady-state measurements are shown. In the upper panel the spectral overlap between donor emission and acceptor absorbance is shown. Middle and lower panels show quenching of the donor emission in the presence of the acceptor in CHT excluded and included RM, respectively. Estimated parameters are given in Tables 1 and 2.

Table 1
Energy transfer from C500 (donor) to various acceptors in α -chymotrypsin excluded reverse micelle: steady-state measurement

Acceptor	Overlap integral ($M^{-1} cm^{-1} nm^4$)	F_{DA}/F_D	R_0 (Å)	R^S (Å)
R123	1.99×10^{15}	0.061	48.97	31.08
EtBr	2.46×10^{14}	0.206	34.56	27.59
Mc540	2.74×10^{15}	0.141	51.65	38.23

Table 2
Energy transfer from C500 (donor) to various acceptors in α -chymotrypsin included reverse micelle: steady-state measurement

Acceptor	Overlap integral ($M^{-1} cm^{-1} nm^4$)	F_{DA}/F_D	R_0 (Å)	R^S (Å)
R123	2.11×10^{15}	0.028	50.20	27.74
EtBr	2.50×10^{14}	0.471	35.18	34.52
Mc540	2.64×10^{15}	0.353	52.12	47.10

sities of the donor in the absence and presence of the acceptor, is higher than that in the RM with CHT (Table 2). The estimated donor–acceptor distances from steady-state experiments in the RM without and with CHT are 31.08 and 27.74 Å, respectively. Note that in the case of R123 there is a huge disagreement of the donor–acceptor distances measured from steady-state and time-resolved experiments, which will be discussed later.

The spectral overlap of the donor C500 and cationic acceptor EtBr is shown in the upper panel of Fig. 3. EtBr is a well-known fluorescent probe for DNA, which readily intercalates into the DNA double helix. Compared to the case of bulk water, the emission intensity and lifetime of EtBr increase nearly 11 times when EtBr intercalates into the double helix of DNA. This remarkable fluorescence enhancement of EtBr is utilized to study the motion of DNA segments. The photophysical processes of the fluorescence enhancement have recently been explored [18]. The selective accumulation of the acceptor in the aqueous phase of the RM comes from the specific nature of the solubility of EtBr; it is completely insoluble in isoctane and highly soluble in the bulk water. The fluorescence quenching effects of the donor C500 in the RM without and with CHT by the acceptor EtBr are shown in the middle and lower panels of Fig. 3, respectively. In the case of RM without CHT (Table 1) the quenching efficiency, F_{DA}/F_D , is lower than that in the RM with CHT (Table 2). The estimated donor–acceptor distances from steady-state experiments in the RM without and with CHT are 27.59 and 34.52 Å, respectively.

Fig. 4, upper, shows spectral overlap of the donor C500 emission and acceptor MC540 absorption spectra. MC540 is an anionic lipophilic polymethine dye, which readily binds to biomembranes, micelles, and proteins. In aqueous solutions, the fluorescence intensity of MC540 increases by an order of magnitude on binding to these biological systems. Further, leukemia cells stained with MC540 are rapidly destroyed on irradiation by light. The photophysical processes

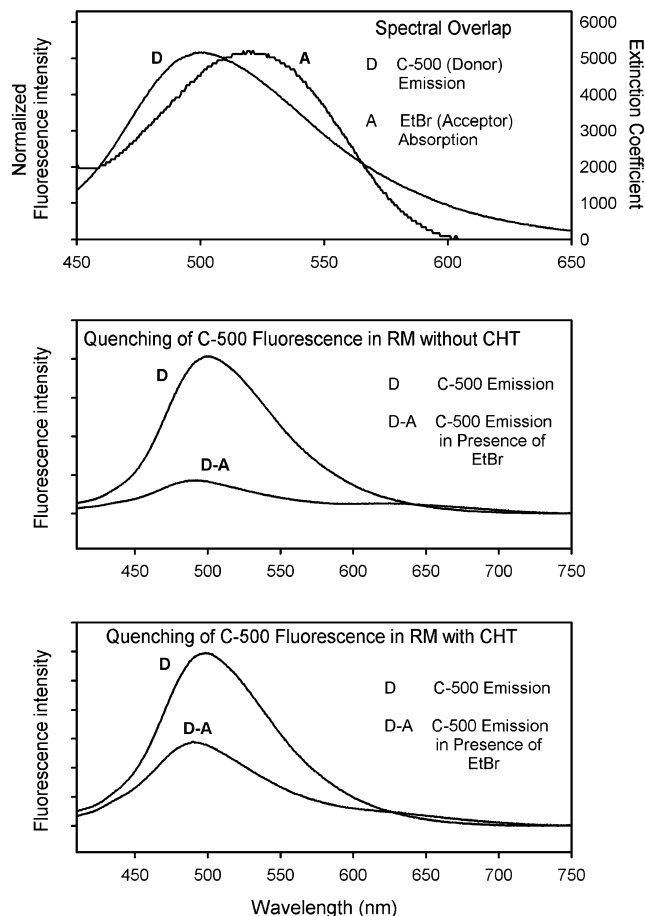


Fig. 3. The fluorescence energy-transfer processes of C500 (donor) to a cationic acceptor EtBr in the RM as evidenced from steady-state measurements are shown. In the upper panel the spectral overlap between donor emission and acceptor absorbance is shown. Middle and lower panels show quenching of the donor emission in the presence of the acceptor in CHT-excluded and -included RM, respectively. Estimated parameters are given in Tables 1 and 2.

of the fluorescence enhancement have recently been explored [19]. The selectivity of the acceptor to the aqueous phase of the RM comes from the specific nature of the solubility of MC540; it is completely insoluble in isoctane and highly soluble in bulk water. The significantly large overlap facilitates quenching of the donor in the donor–acceptor system in RM without and with CHT as shown in the middle and lower panels of Fig. 4, respectively. In the case of RM without CHT (Table 1) the quenching efficiency, F_{DA}/F_D , is lower than that in the RM with CHT (Table 2). The estimated donor–acceptor distances from steady-state experiments in the RM without and with CHT are 38.23 and 47.10 Å, respectively.

From the steady-state quenching studies of the donor C500 it has been revealed that upon inclusion of CHT in the RM the donor–acceptor distances for EtBr and MC540 increase. However, in the case of R123, the more efficient quenching of the donor reveals the donor–acceptor distance in the case of CHT-included RM to be lower than that in RM without CHT. This observation is not in agreement with

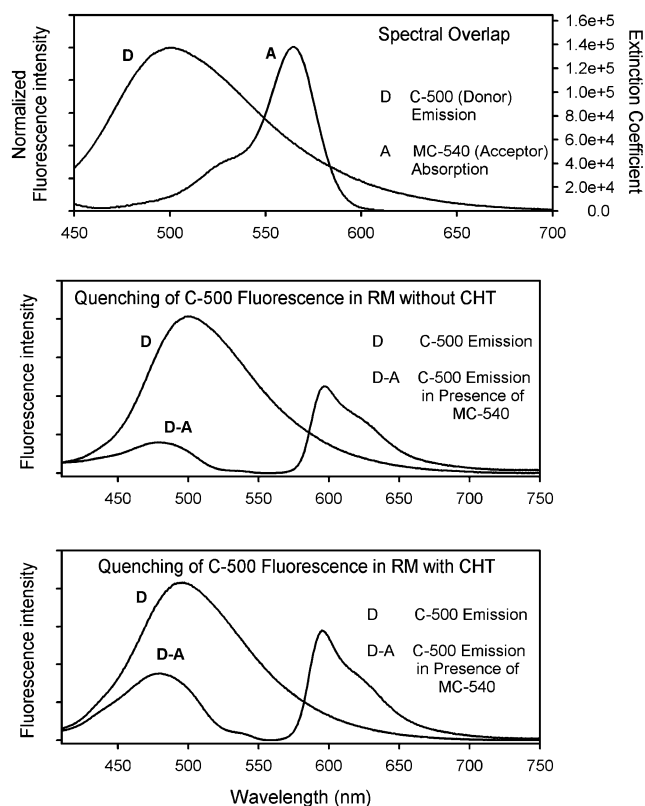


Fig. 4. The fluorescence energy-transfer processes of C500 (donor) to an anionic acceptor MC540 in the RM as evidenced from steady-state measurements are shown. In the upper panel the spectral overlap between donor emission and acceptor absorbance is shown. Middle and lower panels show quenching of the donor emission in presence of the acceptor in CHT-excluded and -included RM, respectively. Estimated parameters are given in Tables 1 and 2.

the time-resolved studies, as discussed in the following section. The absolute intensity of C500 in the CHT-included RM, as shown in the middle panels of Figs. 2–4 should not be compared with that in the RM with CHT (lower panels of Figs. 2–4), because the experimental condition, namely optical density of the probe C500, in the above two cases was different. However, the steady-state quenching efficiency (F_{DA}/F_D) does not depend on its absolute intensity. In the cases of the donor–acceptor systems of R123 and MC540, the acceptors show large emission intensities, as shown in Figs. 2 and 4, respectively. These emissions are not due to the direct excitations of the acceptors, because in the excitation wavelength (400 nm) the acceptors offer negligibly small optical absorptions. The enhanced emissions from the acceptors are the indications of energy-transfer processes in the RM. In the buffer solution the steady-state spectroscopic studies (absorption, emission, and anisotropy; data not shown) did not reveal any indication of complexation of the acceptors with CHT. However, the possibility of some specific interactions of the acceptor molecules with the RM-encapsulated CHT cannot be completely ruled out for the following reasons. First, the proximities of the acceptors to CHT in the RM are much higher than those in

the bulk buffer. Second, hydrophobic/charge interactions of CHT with the acceptors could be different from those in the buffer because of the spatial distribution of pH of the aqueous medium in the RM [18]. Nevertheless, our time-resolved anisotropy studies, which reflect the spatial restriction on the acceptor molecules (see below) in the CHT included/excluded RM, indicate negligibly small interactions of the acceptor molecules with CHT upon encapsulation in the RM. Thus within the structural integrity of the enzyme in the RM, it is most expected that in the CHT-included RM, acceptors reside in the interstitial space between the enzyme surface and the inner surface of the RM.

3.2. Time-resolved studies

3.2.1. Solvation and rotational dynamics of the donor at the reverse micellar surface

In order to explore the local environmental rigidity and its change upon inclusion of the enzyme CHT, we studied solvation dynamics of the RM by using the donor as probe in absence and presence of CHT. Fig. 5 (upper) shows the picosecond-resolved transients of the donor C500 in the RM without CHT at three characteristic wavelengths. For solvation dynamics studies a series (at least seven) of systematic wavelengths were taken. The signal initially decays with time constants 200 ps and 1.0 ns at the blue side (~ 425 nm) of the fluorescence spectrum but rises with the similar time constant at the red side (~ 625 nm). A decay component for all wavelengths was found with a time constant of ~ 5 ns as shown in Fig. 5, upper. The slower 5-ns component is the fluorescence lifetime of the probe C500 in the microenvironment.

The constructed time-resolved emission spectra (TRES) are shown in Fig. 5, lower. The steady-state spectrum of C500 in the RM is also shown for comparison (dotted line). The solvation correlation function $C(t)$ (Fig. 6) shows single-exponential decay with time constant 645 ps; any sub-50-ps components in these dynamics are unresolved. The net spectral shift ($\Delta\nu$) is 1889 cm^{-1} from $21,755$ to $19,866\text{ cm}^{-1}$ (up to 3.0 ns). The anisotropy $r(t)$ of the donor is shown in the inset of Fig. 6. The measured $r(t)$ decays with time constants 210 ps (36%) and 1.2 ns (51%) resulting a persistence (13%) of $r(t)$ in our experimental window (up to 10 ns). The value of $r(t)$ at $t = 0$ is found to be 0.39.

Fig. 7, upper, shows picosecond-resolved transients of the donor C500 in the CHT-included RM. On the blue edge of the fluorescence spectrum the signals decay with time constants (240 ps–1.1 ns) depending on wavelengths, whereas on the red edge the signals are seen to rise (time constant up to 1.1 ns). A decay component, of time constant 5 ns, reflective of the lifetime of the probe, is present in all wavelengths detected (Fig. 7, lower). Fig. 7, lower, shows TRES (up to 3.0 ns) of the donor in the CHT-included RM. The dotted spectrum indicates the steady-state spectrum of the donor. The $C(t)$ function in Fig. 8 can be fitted to a single-exponential decay with time constant 668 ps; any sub-50-ps

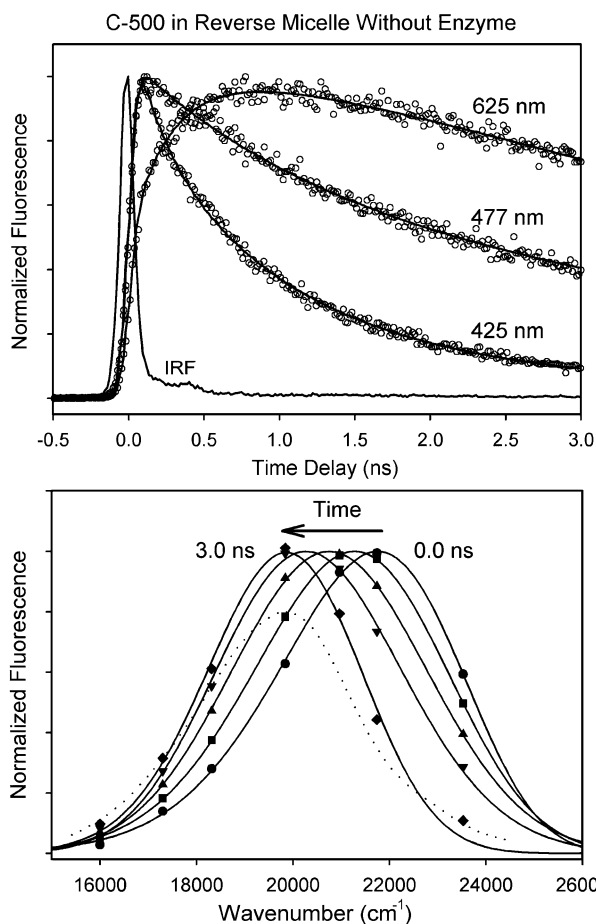


Fig. 5. In the upper panel picosecond-resolved transients of the C500 in the CHT-excluded RM are shown at three characteristic wavelengths. Note the decay in the blue edge (425 nm) and the rise in the red edge (625 nm) of the emission spectrum. Solid lines show numerical fitting of those transients. Instrument response function (IRF) is also shown. The transients are normalized for comparison. Lower panel shows time-resolved emission spectra (TRES) of C500 in the RM. The steady-state spectrum of the sample is also shown for comparison (dotted line). Note that the emission maximum at time 3 ns is similar to that of the steady-state emission.

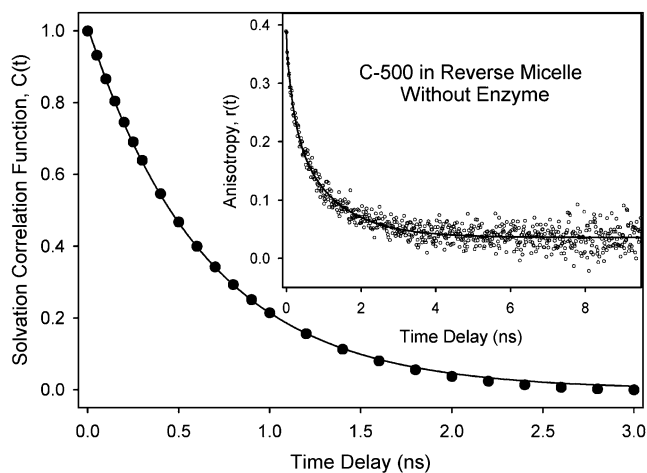


Fig. 6. The solvation correlation function $C(t)$ of C500 in the CHT-excluded RM. Inset shows the time-resolved anisotropy, $r(t)$, of C500 in the same system. Numerical fitting parameters are given in Table 3.

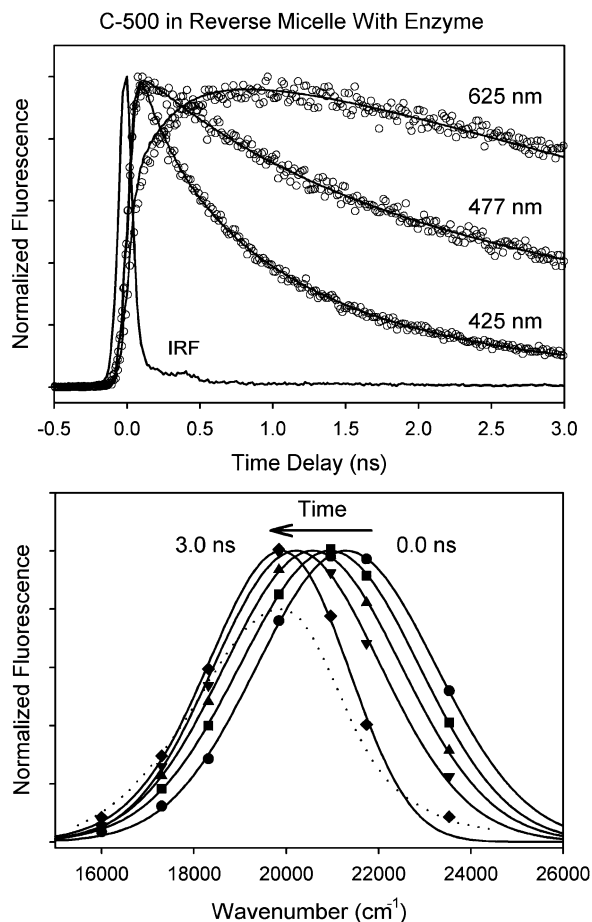


Fig. 7. In the upper panel picosecond-resolved transients of the C500 in the CHT-included RM are shown at three characteristic wavelengths. Note the decay in the blue edge (425 nm) and the rise in the red edge (625 nm) of the emission spectrum. Solid lines show numerical fitting of those transients. Instrument response function (IRF) is also shown. The transients are normalized for comparison. Lower panel shows time-resolved emission spectra (TRES) of C500 in the RM. Steady-state spectrum of the sample is also shown for comparison (dotted line). Note that the emission maximum at time 3 ns is similar to that of the steady-state emission.

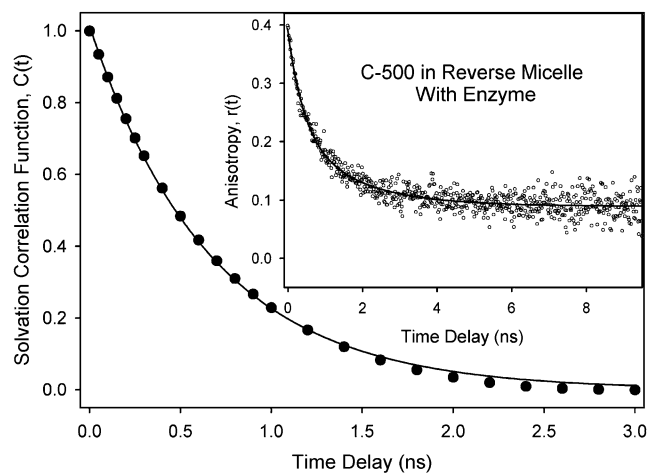


Fig. 8. Solvation correlation function, $C(t)$, of C500 in the CHT-included RM. Inset shows the time-resolved anisotropy, $r(t)$, of C500 in the same system. Numerical fitting parameters are given in Table 3.

components in these dynamics are unresolved. The net spectral shift is 1412 cm^{-1} from $21,301$ to $19,889\text{ cm}^{-1}$ (up to 3.0 ns), which is similar to that of the RM without CHT. As shown in the inset of Fig. 8, the fluorescence anisotropy $r(t)$ at 500 nm decays exponentially with time constants of 434 ps (44%) and 1.7 ns (33%). In contrast to the RM without CHT, the anisotropy at $t = 0$ (0.4) and relatively large residual anisotropy (23%; up to 10 ns) reveal slower rotational dynamics of the probe in the RM upon inclusion of the enzyme CHT.

3.2.2. Heterogeneity in the local environments of the donor

To investigate possible interference of emission from various excited species, we further use a time-resolved area-normalized emission spectroscopic (TRANES) technique developed recently [15]. TRANES is a model-free modified version of TRES mentioned above. Fig. 9 shows TRANES spectra of the donor in the RM without (upper) and with CHT (lower). An isoemissive point at $21,000\text{ cm}^{-1}$ is clearly evident in the spectra of both the samples. One of the possible reasons for the existence of two emissive species in the excited state is due to the solubilization of the C500 chromophore in two different sites of the RM [15]. In other

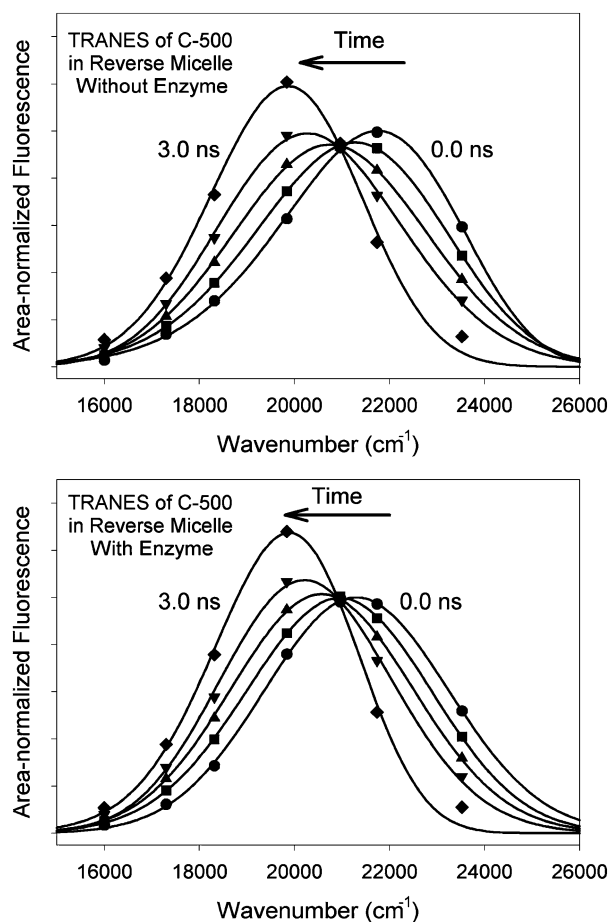


Fig. 9. Time-resolved area-normalized spectra (TRANES) of C500 in the CHT-excluded (upper) and in the CHT-included (lower) RM. Note the isoemissive points at $21,000\text{ cm}^{-1}$ for both systems (see text).

words, the environments around the donor in the RM are heterogeneous.

3.2.3. Diffusion of the probe donor through various environments: emission linewidth analysis

The full width at half maximum (linewidths Γ) of emission spectra of the C500 probe (Fig. 1, lower) were observed to be different in various environments. It increases upon changing the polarity of the immediate environment of C500. In the RM, $w_0 = 10$, the emission linewidth of C500 is larger than that in pure isooctane. The linewidth of emission of C500 in the RM is also very sensitive to inclusion of the enzyme CHT. In the RM without CHT the magnitude of the Γ (3845 cm^{-1}) is larger than that in the CHT-included RM (3606 cm^{-1}). The observation is consistent with the fact that in the polar environment, the fluorescence spectrum of a solute (C500) with a higher excited-state dipole moment compared to that in the ground state is the superposition of emission from different excited states of diverse degrees of solvation [14]. The broadening of emission spectrum may also be indicative of spatial microheterogeneity of the immediate environment of the probe C500 [20–22].

The linewidth (Γ) of TRES (Fig. 10) of C500 in the RM is found to vary with time, which is an evidence of change in local environment during solvation. In the RM without CHT (Fig. 10) $\Gamma(t)$ exhibits a relatively faster rise and a slower decay with time constants 322 ps and 1.6 ns , respectively. The amplitudes of the rise and decay components of linewidth ($\Delta\Gamma$) are 342 cm^{-1} (up to 400 ps , from 4426 to 4768 cm^{-1}) and 1010 cm^{-1} (up to 3.0 ns , from 4768 to 3758 cm^{-1}), respectively. For the CHT-included RM, $\Gamma(t)$

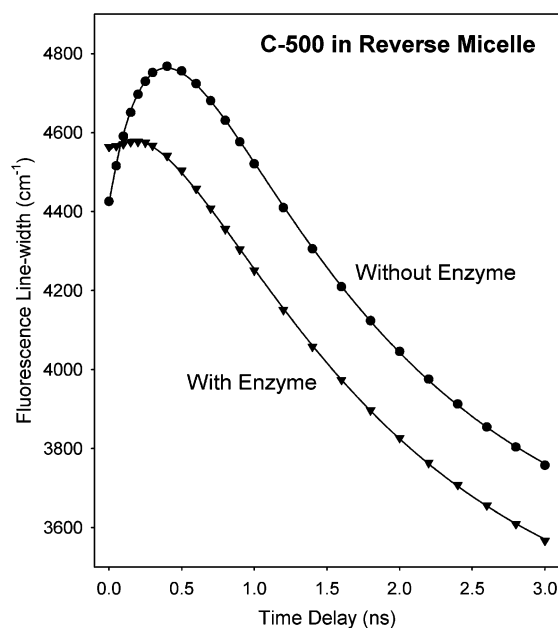


Fig. 10. Time-resolved linewidths (Γ) of TRES of C500 in the RM without (up) and with (down) the enzyme CHT are shown. Note the significantly large amplitude of the rise component in the linewidth with time for the RM without CHT compared to that in the RM with CHT.

Table 3
Numerical fitting parameters of the time-resolved solvation and anisotropy of donor and donor–acceptor systems in the RM

Reverse micelle	Emission maximum (nm)	Solvation correlation function, $C(t)$	Rotational anisotropy, $r(t)$
α -Chymotrypsin excluded	500	Single exponential decay $\tau = 645$ ps $\Delta\nu = 1889$ cm^{-1}	$r_0 = 0.39$ $\tau_1 = 0.21$ ns, $A_1 = 36\%$ $\tau_2 = 1.2$ ns, $A_2 = 51\%$ Residual $r(t) = 13\%$
α -Chymotrypsin included	500	Single exponential decay $\tau = 668$ ps $\Delta\nu = 1412$ cm^{-1}	$r_0 = 0.40$ $\tau_1 = 0.43$ ns, $A_1 = 44\%$ $\tau_2 = 1.7$ ns, $A_2 = 33\%$ Residual $r(t) = 23\%$

shows similar temporal characteristics; however, the amplitude of the rise component is much smaller than former case. In the latter case the amplitudes of the rise (time constant 410 ps) and decay (time constant 1.6 ns) components of linewidth ($\Delta\Gamma$) are 13 cm^{-1} (up to 200 ps, from 4564 to 4577 cm^{-1}) and 1010 cm^{-1} (up to 3.0 ns, from 4577 to 3567 cm^{-1}), respectively.

From the studies of time-dependent spectral width an interesting feature of the relaxation dynamics of C500 in the RM is evident. In the case of the RM without CHT, the rise with time constant 322 ps is indicative of diffusion of the probe from the surface of the RM to the polar aqueous and nonpolar isooctane phases of the RM making the spatial environments of the donor more heterogeneous with time. After certain time (up to 400 ps), the probe is expected to cross the aqueous phase and again face the nonpolar isooctane medium offering relatively homogeneous environments, as evidenced by the decay of the $\Gamma(t)$. Taking the diffusion constant of an organic probe at the micellar surface to be 15.3 $\text{\AA}^2/\text{ns}$ [23], the estimated distance traversed by the probe in 400 ps is 3.5 \AA . This is much shorter than the diameter of the RM (40 \AA) at $w_0 = 10$. Conversely, in the CHT-included RM, the available aqueous phase (shell) for the diffusion of the donor probe is much less than that of the former case. The estimated distance traveled by the donor in 200 ps is 2.5 \AA . As indicated by the magnitude of the rise, the population of the donor molecules in this journey is significantly lower than in former case of RM without CHT. The similarity in the amplitudes and time constants of the decay components for both the cases is not surprising, given the fact that these decays are associated with the diffusion of the donor in the nonpolar isooctane medium.

3.2.4. Fluorescence resonance energy transfer of the donor in the RM

In Fig. 11 the transients of the donor C500 without and with different acceptors in the RM in the absence of CHT are shown. As shown in Tables 4 and 5, the fluorescence transient of the donor in the RM shows a fast rise (time constant 200 ps), indicating solvation, followed by a decay of time constant 5.0 ns, which is the lifetime of the donor in the microenvironment. In the presence of the acceptor R123, time-resolved fluorescence shows biexponential decay of time

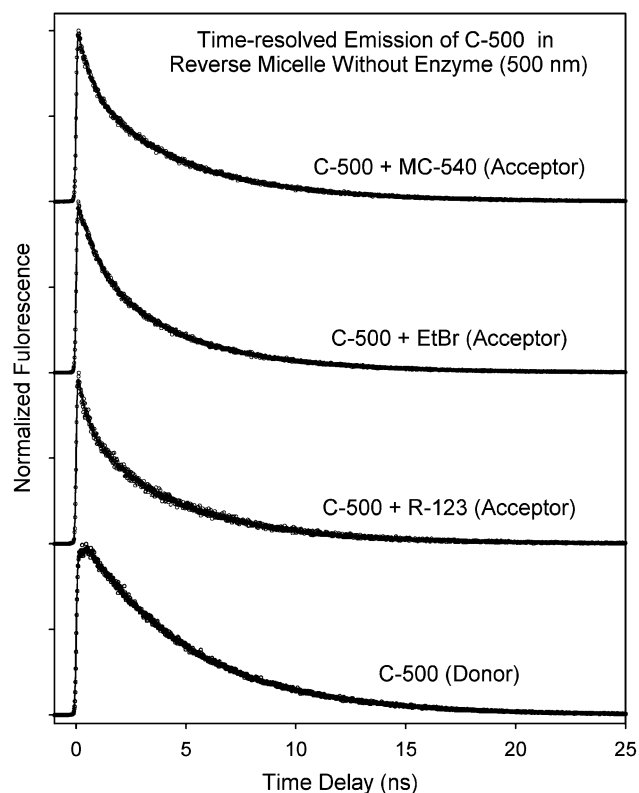


Fig. 11. Time-resolved transients of the donor (C500) in the CHT-excluded RM in the absence and presence of various acceptor molecules are shown. All the transients were taken at 500 nm and normalized for comparison. Numerical fitting parameters are given in Table 4.

constants 500 ps (35%) and 4.5 ns (65%). The persistence of the longer lifetime (4.5 ns, 65%) distinctly indicates that in the donor–acceptor system only 35% of the donor population is undergoing an energy-transfer process [16]. The estimated donor–acceptor distance is 33.98 \AA . From the biexponential transient of time constants 1.1 ns (40%) and 4.6 ns (60%) of the C500–EtBr system in the RM it is evident that 40% of the donor population is responsible for the energy transfer, with an average distance of 27.94 \AA from the acceptor EtBr. In the case of the C500–MC540 system the biexponential decay of the donor fluorescence reveals two time constants of 720 ps (35%) and 4.7 ns (65%). This indicates that 35% of the donor molecules in the RM transfer their energy to ac-

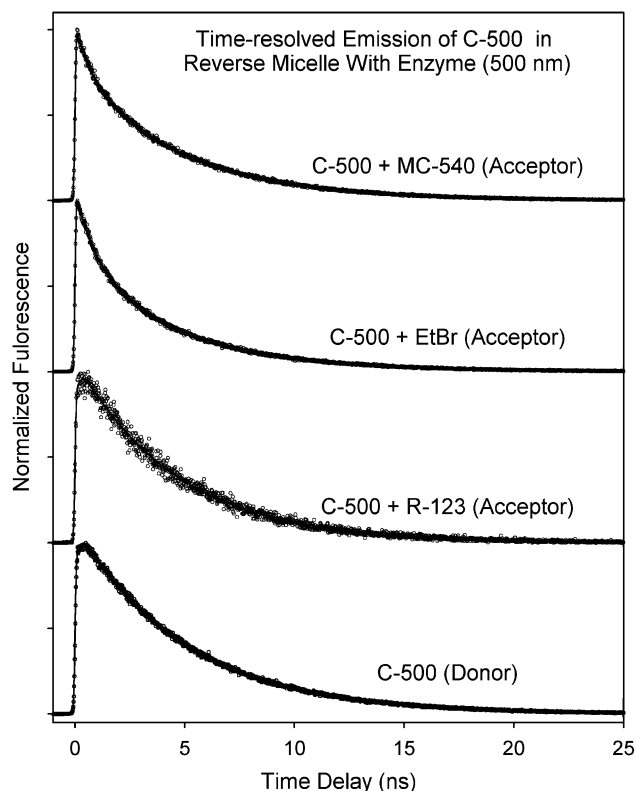


Fig. 12. Time-resolved transients of the donor (C500) in the CHT-included RM in the absence and presence of various acceptor molecules are shown. All the transients were taken at 500 nm and normalized for comparison. Numerical fitting parameters are given in Table 5.

ceptors at an average distance of 38.37 Å. The efficiency of the energy transfer for various donor–acceptor systems and estimated average donor–acceptor distances is summarized in Table 4. All estimated distances in the RM without CHT are less than the diameter of the water pool (40 Å) of the RM at $w_0 = 10$.

Fig. 12 shows fluorescence transients at 500 nm of the donor C500 in the CHT-included RM in the absence and presence of various acceptors. The fluorescence transient of the donor in this case shows a fast rise (time constant 200 ps), indicating solvation, followed by a decay of time constant 5.0 ns, which is the lifetime of the donor in the RM. In the presence of the acceptor R123 a significant quenching of the emission of the donor is evidenced by steady-state measurement (Fig. 2) and also by the poor signal-to-noise ratio of the acquired transient (Fig. 12, second from bottom). However, the transient is similar to that of the donor in absence of the acceptor, indicating the quenching to be reflective of a radiative mechanism of energy transfer (reabsorption by the acceptor), *not* the resonance type. In contrast to the former case, the lack of coexistence of donor and acceptor in the CHT-included RM is the possible reason for the radiative energy transfer mechanism. The disagreement of the estimated donor–acceptor distances from steady-state (Table 2) and time-resolved studies (Table 5) warrant a potential danger of using the former as a conclusive experiment to

Table 4
Numerical fitting parameters of the transients of donor and donor–acceptor systems in the CHT-excluded RM

System	a_1 (%)	τ_1 (ns)	a_2 (%)	τ_2 (ns)	τ_{DA}/τ_D	R^{TR} (Å)
Donor	–32	0.2	132	5.0	–	–
Donor–acceptor						
R123	35	0.5	65	4.5	0.100	33.98
EtBr	40	1.1	60	4.6	0.218	27.94
MC540	35	0.72	65	4.7	0.144	38.37

Table 5
Numerical fitting parameters of the transients of donor and donor–acceptor systems in the CHT-excluded RM

System	a_1 (%)	τ_1 (ns)	a_2 (%)	τ_2 (ns)	τ_{DA}/τ_D	R^{TR} (Å)
Donor	–28	0.2	128	5.0	–	–
Donor–acceptor						
R123	–30	0.2	130	4.9	~1	–
EtBr	38	1.0	62	4.7	0.200	27.92
MC540	26	0.76	74	4.8	0.152	39.14

measure donor–acceptor distance by using the energy transfer mechanism in chemical and biological systems. From the biexponential transient of time constants 1.0 ns (38%) and 4.7 ns (62%) of the C500–EtBr system in the RM, it is evident that 38% of the donor population is responsible for the energy transfer with an average distance of 27.92 Å from the acceptor EtBr. In the case of the C500–MC540 system the biexponential decay of the donor fluorescence reveals two time constants of 760 ps (26%) and 4.8 ns (74%), which indicate that 26% of the donor molecules in the RM transfer their energy to acceptors at an average distance of 39.14 Å. The estimated distances are similar to that in the RM without CHT, except for the acceptor R123, where the distance is too large to have resonance-type energy transfer in the CHT-included RM.

3.2.5. Local environmental restriction on the acceptors

In order to explore the local geometric restriction of the microenvironment on the physical motions of the acceptors in the RM without and with CHT, we performed time-resolved anisotropy studies ($r(t)$) of the acceptors. In these studies we excited the donor molecule and measured the anisotropy at the peak wavelengths of the acceptor molecules. In the CHT-excluded (Fig. 13) and -included (Fig. 14) RM fluorescence anisotropy decays of the acceptors ($r(t)$) could be described by biexponential functions. The time constants, relative amplitudes, and residual anisotropy values are shown in Table 6. The fast depolarization components can be attributed to the local tumbling motions of the acceptors. The slow component, which is similar to that of the donor molecules in the corresponding RM, can be assigned tentatively to a rotation of the whole molecule and/or to global rotational motion of the RM.

The similarity in the transients of anisotropy of the acceptor molecules in the CHT-included RM with that in the

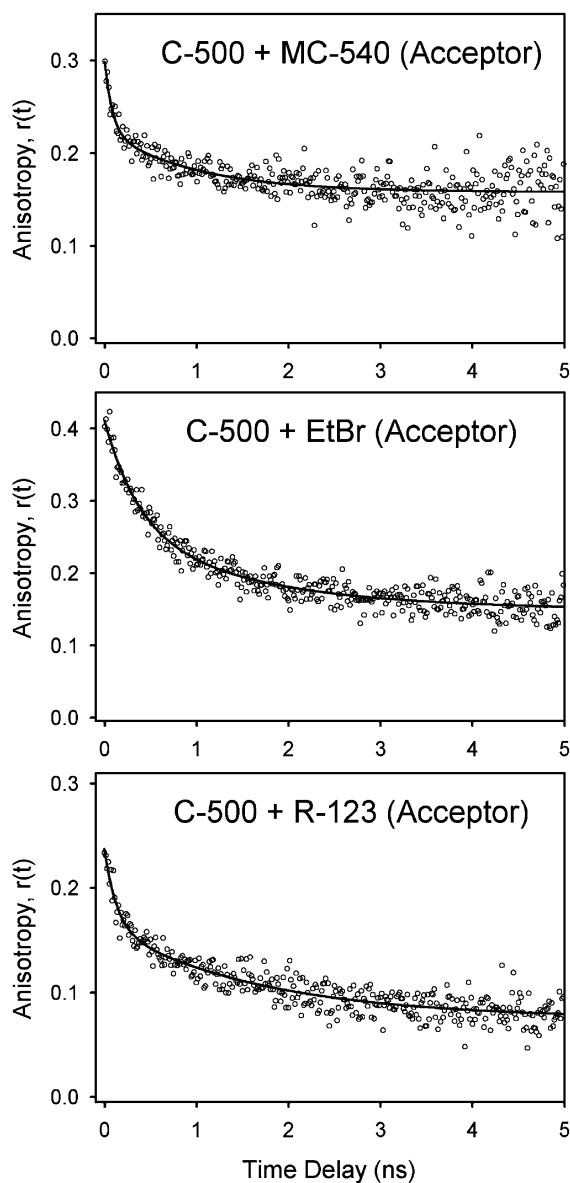


Fig. 13. Time-resolved anisotropies of the acceptor molecules, MC540 (upper), EtBr (middle), and R123 (lower), in the CHT-excluded RM are shown. Note that acceptors were excited indirectly (via donor). Numerical fitting parameters are given in Table 6.

RM without CHT is reflective of an analogous geometrical restriction on the acceptors in the microenvironments. This observation is consistent with the fact that the interactions of acceptor molecules with CHT in the RM are not significant. Note that the anisotropy values at $t = 0$ (r_0) and the faster time constants of the acceptor molecules in the CHT-excluded/-included RM may have interference from the energy transfer dynamics from the donor molecule. From the data given in Tables 4, 5, and 6, it is evident that the faster time constants (0.1–0.4 ns) in the anisotropy decays are faster than those of the characteristic time constants of energy-transfer processes (0.2–1 ns) and the slower time constants are comparable in both cases. This observation is consistent with the significant randomization of relative ori-

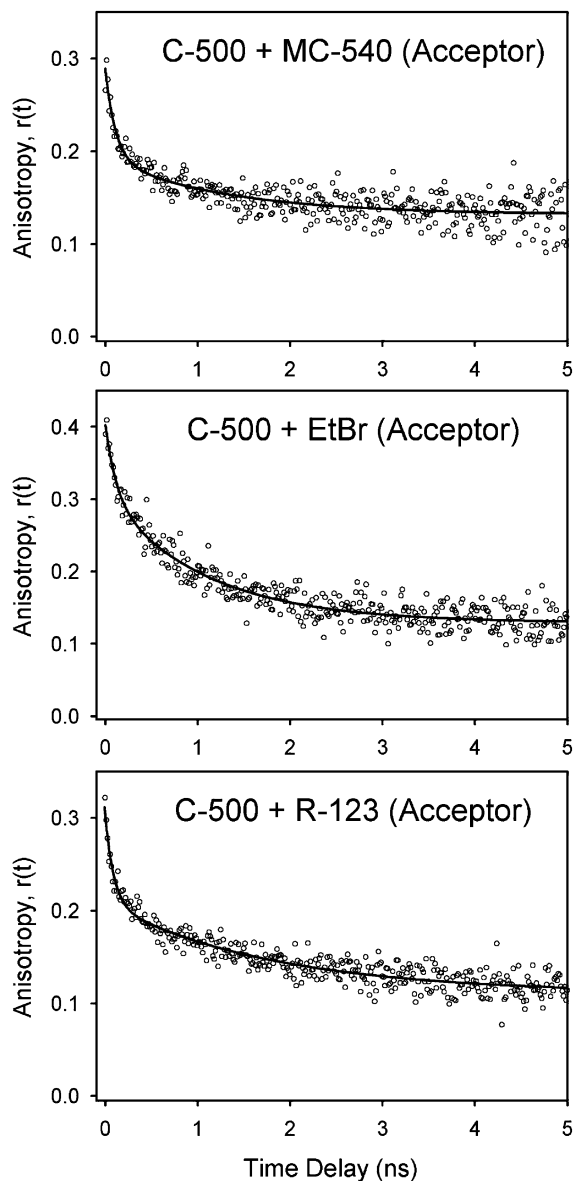


Fig. 14. Time-resolved anisotropies of the acceptor molecules, MC540 (upper), EtBr (middle), and R123 (lower) in the CHT-included RM are shown. Note that acceptors were excited indirectly (via donor). Numerical fitting parameters are given in Table 6.

entation between donor and acceptor molecules prior to or during the energy transfer process.

4. Conclusion

Reverse micelle (RM) is well known as an important chemical and biological medium. The reported studies with picosecond resolution of the donor C500 selectively excited at the surface of a RM elucidate its solvation dynamics and resonance energy transfer in the RM without and with the enzyme α -chymotrypsin (CHT). The enzyme is known to preserve its native structural integrity in the RM with the degree of hydration ($w_0 = 10$) used in our experiment [11].

Table 6
The time-resolved anisotropy of the donor C500 and donor–acceptor systems in reverse micelle

Reverse micelle	Donor (C500)	C500–R123	C500–EtBr	C500–MC540
CHT excluded	$r_0 = 0.39$	$r_0 = 0.23$	$r_0 = 0.40$	$r_0 = 0.30$
	$\tau_1 = 0.21$ ns, $a_1 = 36\%$	$\tau_1 = 0.13$ ns, $a_1 = 30\%$	$\tau_1 = 0.37$ ns, $a_1 = 38\%$	$\tau_1 = 0.10$ ns, $a_1 = 27\%$
	$\tau_2 = 1.2$ ns, $a_2 = 51\%$	$\tau_2 = 1.7$ ns, $a_2 = 40\%$	$\tau_2 = 1.5$ ns, $a_2 = 30\%$	$\tau_2 = 0.98$ ns, $a_2 = 23\%$
	Residual $r(t) = 13\%$	Residual $r(t) = 30\%$	Residual $r(t) = 32\%$	Residual $r(t) = 50\%$
CHT included	$r_0 = 0.40$	$r_0 = 0.30$	$r_0 = 0.40$	$r_0 = 0.27$
	$\tau_1 = 0.43$ ns, $a_1 = 44\%$	$\tau_1 = 0.10$ ns, $a_1 = 30\%$	$\tau_1 = 0.12$ ns, $a_1 = 24\%$	$\tau_1 = 0.11$ ns, $A_1 = 35\%$
	$\tau_2 = 1.7$ ns, $a_2 = 33\%$	$\tau_2 = 1.9$ ns, $a_2 = 32\%$	$\tau_2 = 1.1$ ns, $a_2 = 45\%$	$\tau_2 = 1.3$ ns, $A_2 = 22\%$
	Residual $r(t) = 23\%$	Residual $r(t) = 38\%$	Residual $r(t) = 31\%$	Residual $r(t) = 43\%$

The solvation process of C500 in the CHT-excluded RM was found to be similar to that of the CHT-included RM, giving a single-exponential decay of the solvation correlation function $C(t)$ with a time constant of ~ 660 ps. In contrast, the time-resolved anisotropy ($r(t)$) measurement of the donor in the CHT-included RM shows more geometrical restriction on the donor probe C500 compared to that in the RM without CHT. These observations are consistent with the fact that in the CHT-included RM ($w_0 = 10$) when the diameter of the water pool of the RM is just sufficient to engulf native CHT, the aqueous space (labile type) available to the donor forms an annular shell. The annular aqueous space impose a restriction on the physical motion of the donor C500, as confirmed by $r(t)$ measurement of the CHT-included RM. However, upon inclusion of CHT in the RM the mobility of the solvent molecules in the close vicinity of the donor remains similar as discussed above. The formation of the annular shell like structure in the CHT-included RM is further supported by time-resolved spectral linewidth analysis of the donor revealing its translational diffusion in the RM without and with the enzyme CHT. From the temporal behavior of the diffusion of the donor in the CHT-included RM we estimate the thickness of the annular shell to be ~ 2.5 Å. The effect of this aqueous layer on the structure and functionality of the enzyme CHT included in the RM is extremely important [4,11].

In order to study the change in locations of the hydrophilic acceptor molecules in the RM upon inclusion of CHT and to estimate distances of those acceptors from a donor at the polar surface of the RM, we used steady-state and time-resolved spectroscopic techniques. The estimated donor–acceptor distances from the steady-state fluorescence energy-transfer experiments on the CHT-excluded/-included RM are in close agreement with those of the picosecond-resolved studies except for the acceptor R123. In the case of R123 the estimated donor–acceptor distance measured from the steady-state quenching of donor fluorescence in the CHT-included RM was found to be 27.74 Å. However, the time-resolved transient of C500 in presence of R123 in the CHT-included RM was found to be similar to that of the donor without the acceptor R123, revealing that the energy-transfer mechanism is not of resonance type. It is just reabsorption of the donor emission by the acceptor at a significantly large distance. From these studies it is clearly

evident that EtBr and MC540 rearranged their locations near the surface of the RM upon inclusion of CHT. However, the acceptor R123 has to leave the CHT-included RM in order to create a space for the enzyme. It is worth noting that EtBr and R123 both are cationic dyes but behave quite differently when encapsulated in the RM containing CHT. The proper explanation of the incoherent behavior of R123 compared to that of EtBr demands further investigation and is currently the prime focus of our group. These observations may have significance in understanding the enzymatic reactions of RM-bound CHT with hydrophilic substrates.

The time resolved anisotropy of the acceptor molecules as shown in Fig. 14 (Table 6) reveals biexponential decays with significantly large residual anisotropy (residual $r(t)$), which do not decay within our experimental time window. The longer decay components, which remain similar for both the RM (CHT-included/-excluded), are consistent with those of the donor anisotropies without acceptors, revealing rotational motions of the acceptor molecules as a whole and/or global motion of the RM. The shorter time constants of the $r(t)$ decays could be assigned to the tumbling/segmental motion of the acceptors. Note that indirect excitation of the acceptor molecules (via donor) may have some effect on the anisotropy values at $t = 0$ (r_0). The time-resolved anisotropy of the donor and acceptor molecules revealed significant randomization of the relative orientation of the transition dipoles of the donor and acceptor justifying the value of orientation factor, κ^2 , which is assumed to be 2/3 in this study. Currently we are examining the effect of size of the RM (hydration level) on the solvation and energy-transfer processes of a donor molecule sitting on an enzyme/protein encapsulated in the RM.

Acknowledgments

We thank Professor Sushanta Dattagupta, Director, S.N. Bose National Centre for Basic Sciences, for his continued support, interest, and encouragement. We thank Dr. Nilmoni Sarkar, IIT, Kharagpur, India for his support and help during the time-resolved measurements. We thank Dr. Uday Kumar, S.N. Bose National Centre for Basic Sciences, for his continued interest and helpful comments.

References

- [1] S.K. Pal, A.H. Zewail, *Chem. Rev.* 104 (2004) 2099.
- [2] M.T. de Gomez-Puyou, A. Gomez-Puyou, *Crit. Rev. Biochem. Mol. Biol.* 33 (1998) 53.
- [3] A.V. Levashov, N.L. Klyachko, *Russ. Chem. Bull. Int. Ed.* 50 (2001) 1718.
- [4] R. Biswas, S.K. Pal, *Chem. Phys. Lett.* 387 (2004) 221.
- [5] J.A. Rupley, G. Cateri, *Adv. Protein Chem.* 41 (1991) 37.
- [6] P.L. Luisi, M. Giomini, M.P. Pileni, *Biochim. Biophys. Acta* 947 (1988) 209.
- [7] M.P. Pileni, *Adv. Colloid Interface Sci.* 46 (1993) 139.
- [8] C.M. Carvalho, J.M. Cabral, *Biochimie* 82 (2000) 1063.
- [9] A.M. Klibanov, *TIBS* 14 (1989) 141.
- [10] J.K.A. Kamal, T. Xia, S.K. Pal, L. Zhao, A.H. Zewail, *Chem. Phys. Lett.* 387 (2004) 209.
- [11] A.L. Creagh, J.M. Prausnitz, H.W. Blanch, *Enzyme Microb. Technol.* 15 (1993) 383.
- [12] T.K. De, A. Maitra, *Adv. Colloid Interface Sci.* 59 (1995) 95.
- [13] D.V. O'Connor, D. Philips, *Time Correlated Single Photon Counting*, Academic Press, London, 1984.
- [14] M.L. Horng, J.A. Gardecki, A. Papazyan, M. Maroncelli, *J. Phys. Chem.* 99 (1995) 17,311.
- [15] A.S.R. Koti, M.M.G. Krishna, N. Periasamy, *J. Phys. Chem. A* 105 (2001) 1767.
- [16] J.R. Lakowicz, *Principles of Fluorescence Spectroscopy*, second ed., Kluwer Academic/Plenum, New York, 1999.
- [17] S.D. Bernal, T.J. Lampidis, I.C. Summerhayes, L.B. Chen, *Science* 218 (1982) 1117.
- [18] S.K. Pal, D. Mandal, K. Bhattacharyya, *J. Phys. Chem. B* 102 (1998) 11,017.
- [19] D. Mandal, S.K. Pal, D. Sukul, K. Bhattacharyya, *J. Phys. Chem. A* 103 (1999) 8156.
- [20] P. Dutta, S. Sen, S. Mukherjee, K. Bhattacharyya, *Chem. Phys. Lett.* 382 (2003) 426.
- [21] N.A. Smith, S.R. Meech, I.V. Rubtsov, K. Yoshihara, *Chem. Phys. Lett.* 303 (1999) 209.
- [22] M. Viard, J. Gallay, M. Vincent, M. Paternostre, *Biophys. J.* 80 (2001) 347.
- [23] H.L. Tavernier, F. Laine, M.D. Fayer, *J. Phys. Chem. A* 105 (2001) 8944.